Testing for Erosion-Corrosion Under Disturbed Flow Conditions Using a Rotating Cylinder with a Stepped Surface

S. Nesic, J. Bienkowski, K. Bremhorst, and K.-S. Yang ***

ABSTRACT

Erosion-corrosion is most severe in the vicinity of flow disturbances. In the past, erosion-corrosion under disturbed flow conditions has been studied experimentally in flow loops and numerically by performing flow simulations. In this study, a new, compact experimental setup was tested, intended for the study of erosion-corrosion under disturbed flow conditions, involving a rotating cylinder geometry with a sudden step. A thorough characterization of this new setup was initiated, involving wall mass-transfer measurements complemented with direct numerical simulation of the turbulent flow around it. A large variation of the wall mass-transfer rates behind the step was measured, similar in character to the one obtained in flow through a sudden pipe expansion. Flow simulations have confirmed that this flow geometry will create a qualitatively similar mean flow pattern as observed in a sudden pipe expansion flow involving flow separation and reattachment. Simulations also have shown that there is a large-scale unsteadiness in the turbulent flow structure downstream the step, a fact that might have a significant impact on erosion-corrosion. Further work on characterization of the new electrode involving erosion-corrosion measurements is in progress.

KEY WORDS: erosion-corrosion, flow, rotating cylinder electrode

INTRODUCTION

Single-phase flow affects corrosion in a number of ways. When bare metal surfaces corrode, the effect of flow is manifested through altered mass transfer of species involved in the corrosion reaction. When surface films are present in corrosion, flow can contribute to their removal through dissolution (which is often under mass-transfer control) or by mechanical erosion.[1-2] There are many overlapping terms for this type of corrosion, the most common term being erosion-corrosion, which will be used in the present work.

It is a well-established fact that erosion-corrosion is most severe in the vicinity of flow disturbances. Flow disturbances such as sudden steps, protrusions, bends, etc., give rise to complex flow patterns with increased turbulence levels, mass transfer, and surface stresses.

In the past, erosion-corrosion under disturbed flow conditions has been studied experimentally in flow loops[3] and numerically by performing flow simulations.[4] Experimental studies, while expensive to conduct, offered an insight into the causes of erosion-corrosion. Numerical simulations of the flow (typically using k-ε turbulent flow simulators) were instrumental in the search for links between flow parameters and corrosion. After many arguments, the majority opinion is that high turbulence levels in the vicinity of corroding surfaces contribute to increased erosion-corrosion rates.[3,5-7] In the process of getting to this conclusion, many other concepts

Submitted for publication December 1999; in revised form, June 2000.

* Department of Mechanical Engineering, The University of Queensland, Brisbane, Qld 4072, Australia.
** Department of Mechanical Engineering, Inha University, 253 Yonghyun-Dong, Nam-Ku, Inchon, 402-751, Republic of Korea.

0010-9312/00/000199/$5.00+$0.50/0

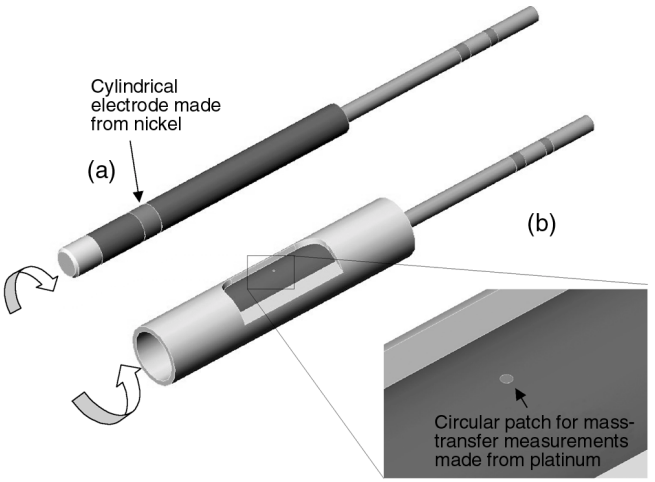

FIGURE 1. *(a) A standard RCE mounted on a shaft and (b) a SRCE.*

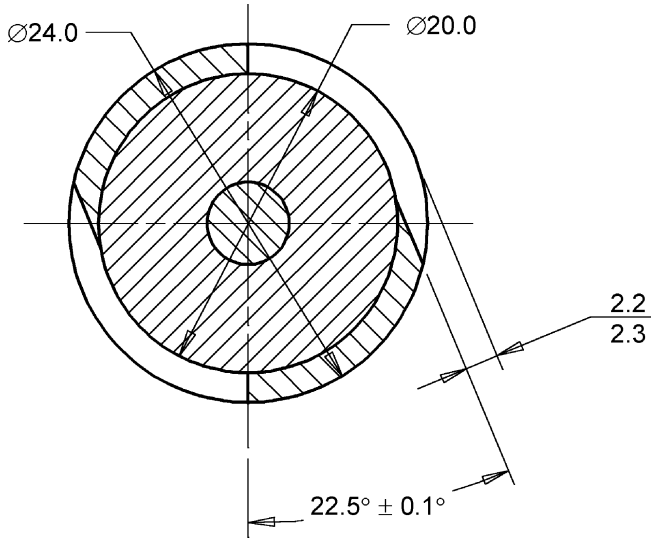

FIGURE 2. *Cross section of the center section of the rotating cylinder with two steps.*

were tested (break-away velocity,[8] critical Reynolds number,[9] mean wall shear stress,[10] etc.) but generally failed.

In most of the experimental studies, it was difficult to distinguish between the above-mentioned flow parameters, because in the case of simple flow patterns found in straight pipe or a rotating cylinder flow, an increase in bulk velocity corresponds to an increase in the Reynolds number and wall shear stress. Higher shear stress creates higher local turbulence levels close to the wall and higher rates of mass transfer and corrosion. It appears that, in such cases, the simplest criterion, a critical or breakaway velocity, is most suitable. However, problems readily arise when results from a simple geometry such as a rotating cylinder, which is a popular system for laboratory studies, are applied to a practical system involving pipe flow. Similar velocities and/or Reynolds numbers in the two systems do not guarantee hydrodynamic and mass-transfer similarity, so the results from different studies are hardly comparable.[5] Thus, use of breakaway velocities and critical Reynolds numbers as integral similarity criteria have to be ruled out. The use of wall shear stress overcomes this problem. Based on the idea that the wall shear stress strips off the protective layer, when its value exceeds the binding force between the film and the base metal, Efird presented a study where he found values for the critical shear stress for flow of seawater in copper-based alloy pipes.[10] This seemed an appealing approach at the time (1977). In addition, the wall shear stress according to the Reynolds analogy of momentum and mass transfer is related to the mass-transfer coefficient. If the assumptions underlying this analogy (Schmidt numbers equal to one and small pressure gradients) are assumed acceptable for particular flow conditions, the proposal that the wall shear stress is related not only to mechanical removal of the protective film but also to the rate of mass transfer,[11] which could affect film dissolution, sounds valid.

Syrett hinted in a 1976 review paper that the degree of fluid turbulence might have a significant effect,[5] which some of the latest studies have shown to be of major importance.[6-7] Actually, in the case of disturbed flow, such as flow through a sudden pipe expansion, it has been noticed that the highest rate of erosion-corrosion is close to the point of flow reattachment.[3] Since the mean wall shear stress is zero at this point, the universal use of the wall shear stress as the sole explanation for removal of the protective film has to be rejected. Based on detailed flow simulations, Nesic and Postlethwaite were able to prove that the local level of near-wall turbulence is at its highest level close to the point of flow reattachment where maximum erosion-corrosion was observed, and suggested that the near-wall turbulence level could be the determining factor.[7] However, the concept of "near-wall turbulence" affecting corrosion still needs clarification and effective means of prediction.

In the present study, a new, compact experimental setup was proposed for study of erosion-corrosion under disturbed flow conditions, involving a rotating cylinder geometry with a sudden step (Figures 1[b] and 2). The authors believe that this geometry can become an effective tool for studying erosion-corrosion under disturbed flow conditions and become a substitution for much more complex and expensive flow loop-based systems.

As the present paper relates to a pilot study, a thorough characterization of the stepped rotating cylinder electrode was initiated and reported, involving wall mass-transfer measurements complemented

with direct numerical simulation (DNS) of the turbulent flow around the electrode.

EXPERIMENTAL PROCEDURES

Electrode

In the past, the standard rotating cylinder electrode system often has been used in electrochemical,[12] mass-transfer,[13-14] and corrosion[15] testing. In most cases, the inner cylinder was rotating; however, in some cases, the measurements involved axial flow or a rotating outer cylinder. In the present investigation, a geometry comprised of a rotating inner cylinder contained within a concentric stationary outer wall was studied. Two variations of the rotating cylinder setup were used in this project:

—A standard rotating cylinder electrode (RCE) consisted of a nickel cylinder mounted on a shaft (Figure 1[a]). The standard RCE system was used to verify that the experimental system behaved in accordance with previously established empirical correlations such as that for mass transfer.[16]

—A stepped rotating cylinder electrode (SRCE) comprised a standard RCE flow geometry, a sleeve used to produce disturbed flow (Figure 1[b]), and a Ø0.7-mm circular platinum patch mounted behind the step. This system was used to investigate the local mass-transfer rates arising from disturbed flow behind the step.

Although, for the purposes of the present investigation, only one step was required on the SRCE for data acquisition. Two steps symmetric with respect to the center of rotation were installed, which allowed the cylinder to be balanced mechanically at all rotational speeds (cross section in Figure 2). The rotating shaft was made from stainless steel covered by a base cylinder and a stepped sleeve, both manufactured from a polytetrafluorethylene (PTFE) material. The cylinder was mounted in a rotator capable of giving accurately controlled rotating speeds up to 10,000 rpm.

When rotated counterclockwise, the rotating cylinder and sleeve arrangement forced flow separation to occur at the step. As a result of this flow separation, it was expected that reattachment and recirculation would occur behind the step. The sleeve was designed so that the distance between the base of the step and the platinum patch in the SRCE could be varied. By changing the relative position of the sleeve to the patch between data acquisition runs, it was possible to obtain mass-transfer measurements behind the step throughout the entire flow-disturbed region. A step height of 2 mm was several orders of magnitude greater than the diffusion sublayer thickness, which is important if enhanced mass-transfer behavior is to be observed in the turbulent flow regime.[17]

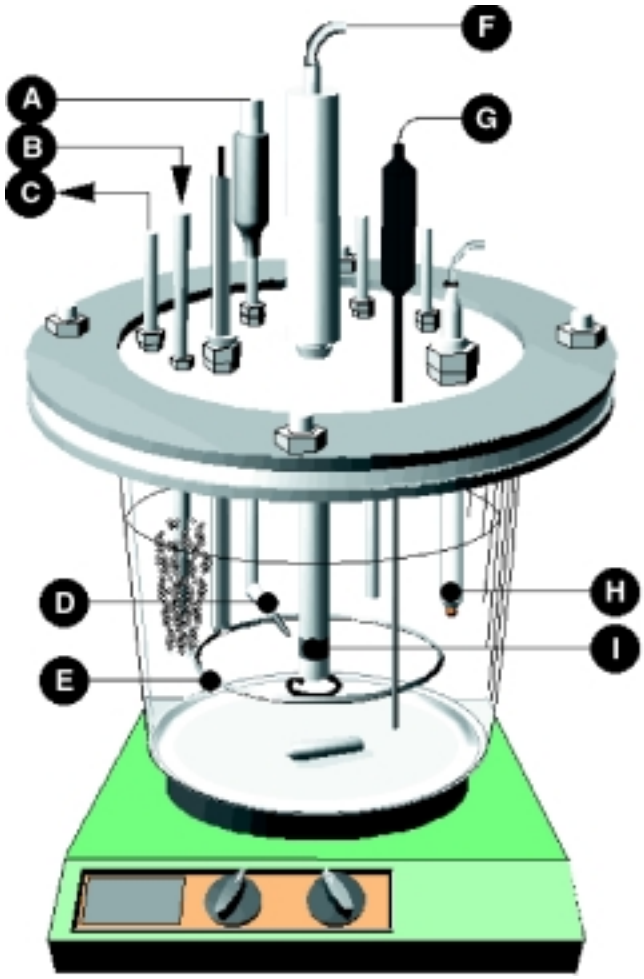

FIGURE 3. *Schematic of a typical experimental test cell: (A) reference electrode, (B) gas in, (C) gas out, (D) Luggin capillary, (E) counter electrode, (F) rotating cylinder, (G) temperature probe, (H) pH electrode, and (I) rotating cylinder and probe.*

Mass-Transfer Measurements

Experimental Setup and Procedures — A three-electrode electrochemical cell was used to make mass-transfer measurements (Figure 3). A saturated silver-silver chloride (Ag-AgCl) reference electrode was used to provide the reference potential (E_{ref}). To minimize the Ohmic drop through the solution, a Luggin capillary was used. The porous wooden tip of the Luggin capillary was placed ≈ 3 mm to 4 mm from the rotating cylinder during data acquisition. The Luggin capillary contained saturated potassium chloride (KCl). The counter electrode consisted of a 80-mm diameter ring manufactured from Ø0.7-mm platinum wire that was placed concentrically around the rotating cylinder.

A potentiostat was used for measurement and control of potential and current during the experiments. An analytical speed controller was used for controlling the rotation of the rotating cylinder. Graphite carbon brushes impregnated with silver

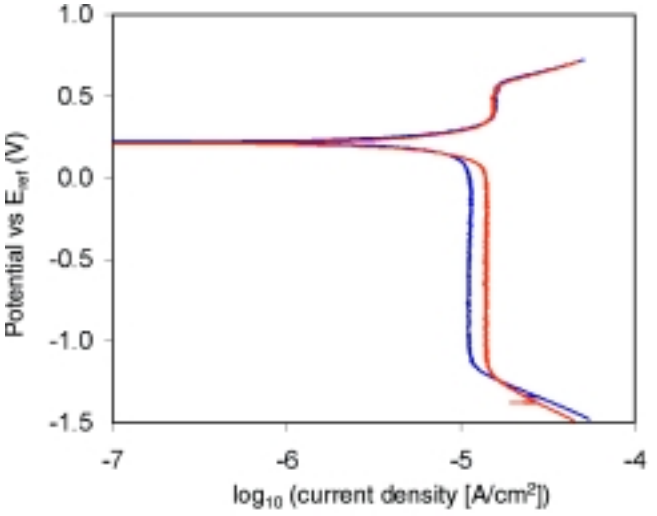

FIGURE 4. *Test of repeatability in experiments with the ferri/ferro cyanide system at 2,000 rpm. The two curves were obtained 5 days apart using the same electrolyte: 0.1 M potassium ferri and ferro cyanide and 0.5 M KOH.*

were used on the motor assembly to connect the probe electrically to the rotating cylinder.

Two different electrode reactions were tested for mass-transfer measurements: oxygen reduction and potassium ferri/ferro cyanide reduction/oxidation. The latter was found to have significantly better repeatability and all mass-transfer results reported were obtained using that electrolyte. It consisted of a deaerated equimolar aqueous solution of ferri and ferro cyanide ($Fe[CN]_6^{3-}$ and $Fe[CN]_6^{4-}$) (ranging between 0.01 M and 0.1 M in different experiments) and 0.1 M to 0.5 M of potassium hydroxide (KOH), which was added as a supporting electrolyte. The ferri/ferro cyanide redox reaction can be represented by:

$$Fe(CN)_6^{3-} + e^- \underset{\text{anode}}{\overset{\text{cathode}}{\rightleftharpoons}} Fe(CN)_6^{4-} \qquad (1)$$

While this reaction is known to afford good reproducibility in different flow geometries,[13,16] certain precautions must be taken. Three problems can arise with the usage of the ferri/ferro cyanide system:

— slow decomposition of the potassium ferro cyanide from exposure to daylight;

— poisoning of the working electrode and counter electrode as a result of hydrogen cyanide (HCN) formation from the above-mentioned decomposition; and

— presence of a considerable amount of oxygen in the cell, which would interfere with the above electrochemical reactions, particularly at low concentrations.

While the exact rate of decomposition of these cyanide complexes has not been quantified in the literature, Eisenberg, et al., suggested that it could be "practically eliminated if the electrolyte was an alkaline solution and kept in darkness," which was found to work reasonably well.[16] Purging with nitrogen practically eliminated oxygen from the solution.

A typical preliminary experiment involved a sweep of the potential 0.5 V above and 1.7 V below the open-circuit potential (E_{oc}) at 5 mV/s. In Figure 4, it is clear that the cathodic reaction offers a broader potential "window" where the limiting current is clearly measurable (nearly 1 V wide) when compared to the anodic reaction (200 mV to 300 mV wide). However, a lack of reproducibility of the cathodic reaction (in magnitude) was observed probably caused by the slow decomposition of the ferro cyanide ion in the presence of light occurring most likely as:

$$Fe(CN)_6^{4-} + 2H_2O \rightarrow Fe(CN)_5H_2O^{3-} + OH^- + HCN \qquad (2)$$

Conversely, the limiting currents associated with the anodic reaction were clearly more reproducible, and they were used in all experiments. Since a potentiostatic technique was used there, the potential was fixed in the middle of the anodic limiting current region. The invariance of this potential window was checked before and after each series of potentiostatic measurements.

Validation of the Mass-Transfer Measurement Technique Using the RCE — Before the stepped rotating cylinder was tested for mass transfer, preliminary experiments were performed to verify the accuracy of the measurement technique by comparison with published data. For fully developed turbulent flow around a standard RCE, the mass-transfer correlation of Eisenberg, et al., is used frequently as a benchmark:[16]

$$Sh = 0.0791\,Re^{0.7}\,Sc^{0.356} \qquad (3)$$

where $Sh = k_m d/D$ is the Sherwood number, k_m is the mass-transfer coefficient in m/s, D is the diffusion coefficient in m^2/s, d is the cylinder diameter in m, $Re = u_\theta d/\nu$ is the Reynolds number, u_θ is the cylinder peripheral velocity in m/s, ν is kinematic viscosity in m^2/s, and $Sc = \nu/D$ is the Schmidt number.

A cylindrical nickel electrode was used (12 mm in diameter and 8 mm in length; Figure 1[a]). A dilute working solution (0.01 M solution of potassium ferri and ferro cyanide, 0.1 M KOH) was selected because of the relatively large surface area of the working electrode. Newman reports that the diffusivity of the ferri cyanide ion at infinite dilution in water at 25°C is 8.96×10^{-10} m^2/s.[12] The temperature correction for the diffusivity can be found by using the Stokes-Einstein equation:

$$D = D_{ref} \times \frac{T}{T_{ref}} \times \frac{\mu}{\mu_{ref}} \quad (4)$$

where D_{ref}, T_{ref}, and μ_{ref} are the fluid properties at the reference temperature of 25°C. For 22°C, which was the solution/room temperature during the experiments, $D = 8.67 \times 10^{-10}$ m²/s, $\mu = 1.1078 \times 10^{-3}$ kg m/s, and $\rho = 1{,}020$ kg/m³, leading to a Schmidt number (Sc = 1,224).

To select an appropriate potential range from which to evaluate the limiting currents, using a potentiostatic technique on a RCE, several sample potentiodynamic scans were taken to observe how the position of the anodic limiting current region varied with the rotational speed (Figure 5). The anodic limiting current region was clearly identifiable for all rotational speeds used. Therefore, the simple mean of the data points between 0.50 V and 0.51 V were used, with respect to Ag-AgCl E_{ref} inclusively (totaling 11 data points for each curve) to evaluate the anodic limiting current.

The measured limiting currents were converted into a mass-transfer coefficient:

$$k_m = \frac{I_{lim}}{n_e F A_e C_b} \quad (5)$$

where I_{lim} is the limiting current in A, n_e is the number of mols of electrons involved in oxidizing/reducing a mol of active species in mol_e/mol, F is the Faraday's constant in C/mol_e, A_e is the working electrode active area in m², and C_b is the concentration of active species in mol/m³.

To maintain generality, results were subsequently nondimensionalized and compared to the correlation of Eisenberg, et al. (Equation [3] in Figure 6).[16] The error bars shown on the plots indicate a 95% window of uncertainty for the parameters indicated on the axes. The original work of Bienkowski details the error analysis.[18] The transitional Reynolds number for flow around a rotating cylinder is 200, which corresponds to a rotational speed of ≈ 30 rpm. All measurements therefore were conducted under turbulent flow conditions.

Results indicated that the measured limiting currents (i.e., mass-transfer rate measurements) correlated well with those predicted by using the Eisenberg, et al., equation.[16] Furthermore, the repeatability of the measurements taken in different occasions and the linearity of the dimensionless plot were highlighted by the correlation coefficient, 0.999. The present measurements were slightly higher than those predicted by the Eisenberg, et al., equation.[16] The magnitude of this difference was of the same order or smaller than the experimental error in the original experiments of Eisenberg, et al.,[16] and therefore was considered acceptable.

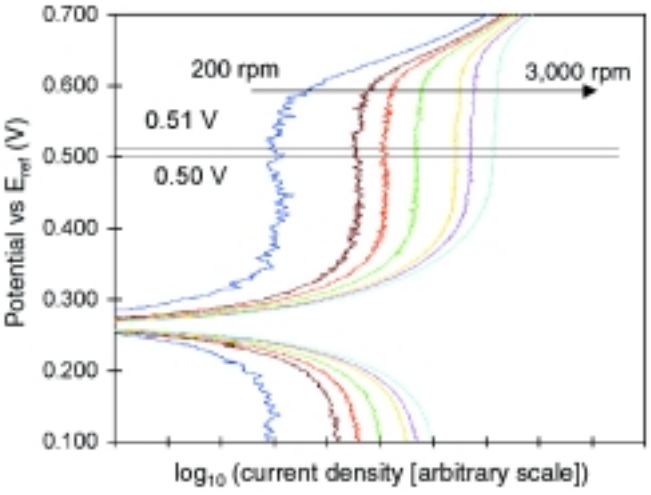

FIGURE 5. *The anodic limiting current potential window on the rotating cylinder electrode for a range of rotation speeds, 200 rpm to 3,000 rpm.*

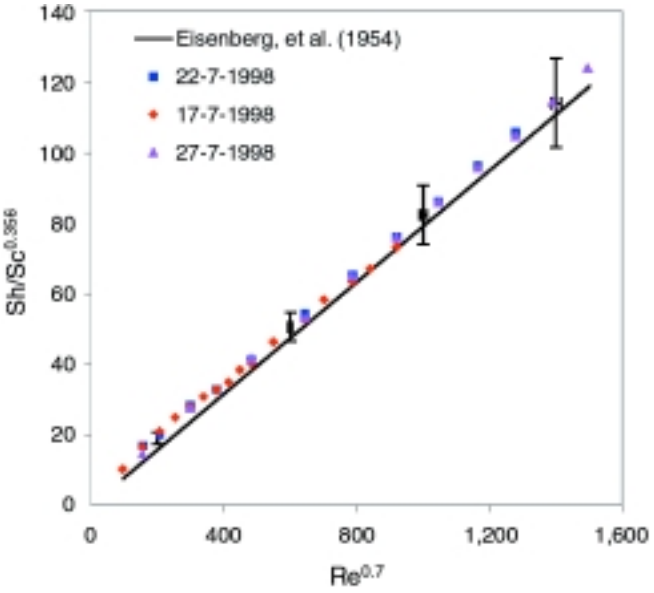

FIGURE 6. *Results of mass-transfer measurements using a standard RCE compared with the Eisenberg, et al., correlation.[16]*

Calibration of the Patch Electrode — To measure the local rates of mass transfer behind the step, a small platinum measuring probe was embedded in the PTFE base surface (Figure 1[b] inset). Since the rest of the surface was electrochemically inactive and since the active platinum patch was so small (Ø0.7 mm in diameter), it was clear that the fully developed mass-transfer boundary layer would not be achieved in the same way as it is on long electrodes or on a standard RCE, which can be seen as an infinitely long electrode. Therefore, the small patch electrode had to be calibrated before each experiment, without the step, to obtain a reference value. A higher concentration of ferro/ferri cyanide

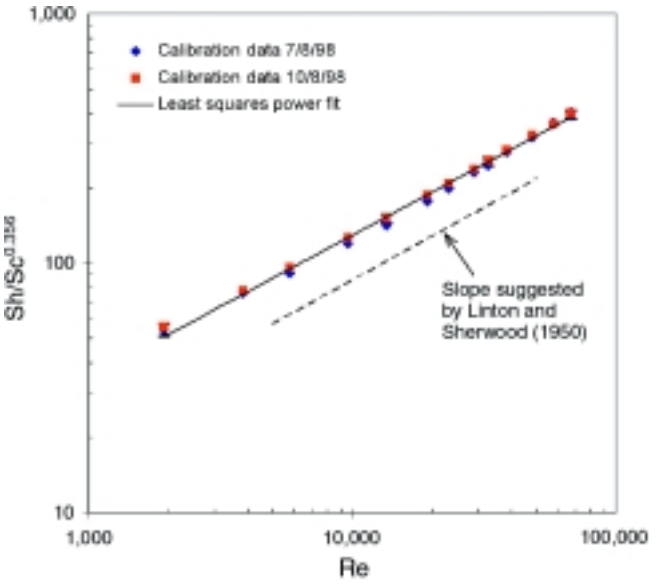

FIGURE 7. *Calibration of the platinum patch electrode obtained using the rotating cylinder geometry without the step.*

(0.1 M) was used to obtain measurable currents on such a small electrode.

A potentiostatic technique was used with a similar procedure as described for the standard RCE. The anodic potential window first was identified using potentiodynamic measurements before each series of potentiostatic measurements. A potential of 0.62 V vs E_{ref} was selected as the middle of this window and maintained in the potentiostatic measurements. The rotational speed was varied between 100 rpm and 3,500 rpm, which corresponds to limiting currents of 100 μA and 740 μA, respectively. For each velocity, the potential stabilized within a few seconds, and subsequently, the final value of the limiting current was taken as an average of 100 points.

Results are plotted in Figure 7 for two series of measurements. The integrated turbulent Leveque equation suggested by Linton and Sherwood[19] predicts a Reynolds number dependence on the mass transfer rate of $Re^{0.583}$ for a developing concentration boundary layer, which is supported by Van Shaw, et al.,[20] who showed that the turbulent convective-controlled mass-transfer rate for a developing boundary layer should depend on $Re^{0.58}$. The present experimental results supported this as points were clustered around a straight line in a log-log plot with a correlation coefficient of 0.9955. The experimentally determined exponent for the Reynolds number dependence of the mass-transfer rate was 0.5734, which is in good agreement with the correlation suggested by Linton and Sherwood.[19] However, in a subsequent calibration, the experimental slope was 0.4968, which highlighted the need for frequent calibrations. Results of these measurements were used as a basis to compare the increase in the mass-transfer rate caused by the presence of the step.

Results of Measurement of Local Mass-Transfer Rates Behind the Step — By changing the position of the platinum patch relative to the sleeve with the step, it was possible to obtain mass-transfer measurements behind the step throughout the entire disturbed flow region. The anodic limiting currents were measured at discrete locations behind the rearward facing step at 200, 500, and 1,000 rpm, corresponding to Reynolds numbers of 3,860, 9,650, and 19,300, respectively, based on the cylinder diameter. Measured mass-transfer rates were normalized with the reference values obtained without the step to obtain the, here-called, mass-transfer enhancement factor as a result of the disturbed flow geometry. Results are plotted in Figures 8 through 10. Error bars shown on the plots indicate a 95% window of uncertainty for the parameters indicated on the axes. Previous work details the error analysis.[18]

The most remarkable feature seen was the large variation of the mass-transfer rates behind the step. The minimum value was ≈ 3 to 4 times smaller, while the maximum was 20% larger than the values obtained on a RCE without the step. These results were similar to the variation obtained downstream a sudden pipe expansion as reported by Sydberger and Lotz.[21] The peak value was located between 2 and 3 step heights downstream the step and seemed to move closer to the step as the Reynolds number was increased. The peak was relatively broad, and there appeared to be an inflexion in the curve somewhere between 4 and 5 step heights downstream the step. While common wisdom and some previous flow simulations suggest that the peak in the mass-transfer rate should be in the vicinity of the reattachment point,[7] this could be clarified only by accurate flow measurements and/or simulations. Because of the size and shape of the flow geometry, detailed measurements of the flow parameters downstream the step were practically impossible. Flow simulations were undertaken and are reported.

The measured variation of the mass-transfer rates behind the step suggests that a complex flow pattern was created using the SRCE, which most likely would lead to a variation in the erosion-corrosion rate.

SIMULATION OF FLOW AROUND A ROTATING CYLINDER WITH A STEP

Formulation

In this study, computations were carried out with respect to a reference frame rotating with a constant angular velocity of the cylinder (Ω). The governing incompressible continuity and momentum equations are:

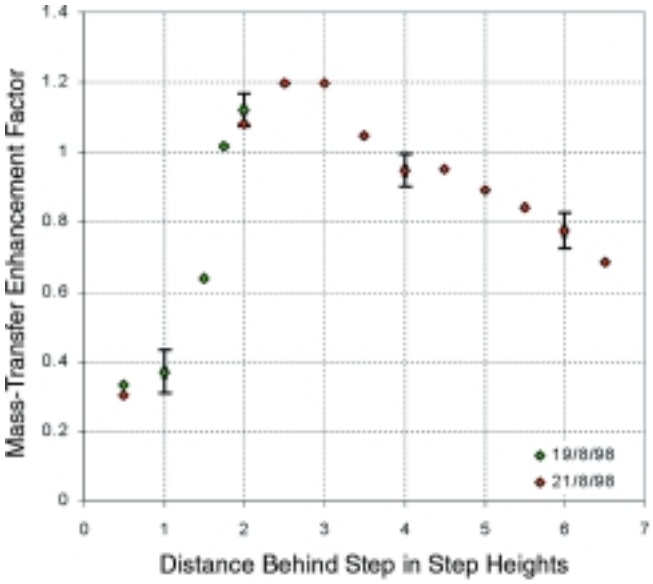

FIGURE 8. *Enhancement of mass transfer behind the step as a function of distance behind the step for 200 rpm (Re = 3,860).*

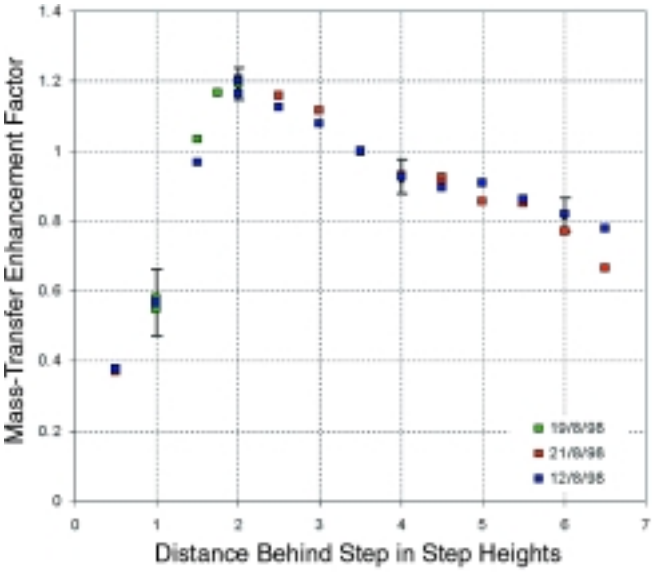

FIGURE 9. *Enhancement of mass transfer behind the step as a function of distance behind the step for 500 rpm (Re = 9,650).*

$$\nabla \bullet u = 0 \tag{6}$$

$$\frac{\partial u}{\partial t} + (u \bullet \nabla)u = -\frac{1}{\rho}\nabla P + \nu\nabla^2 u - 2\Omega \times u \tag{7}$$

where u, ρ, and ν denote velocity vector relative to the rotating reference frame, density, and kinematic viscosity, respectively. The last term in Equation (7) represents the Coriolis force. Since the centrifugal force is conservative, it is included in the pressure term and does not affect the velocity field.[22] Thus, P in Equation (7) includes not only pressure but also the centrifugal potential.

Governing equations were discretized using a finite-volume method in a generalized coordinate system. Spatial discretization was second-order accurate. A hybrid scheme was used for time advancement; nonlinear terms and cross diffusion terms were advanced explicitly by a third-order Runge-Kutta scheme; and the other terms were advanced implicitly by the Crank-Nicolson method. A fractional step method was used to decouple the continuity and momentum equations.[23] Previous work details the numerical algorithm used in the code.[23]

Choice of Numerical Parameters

Simulation of the flow around SRCE was performed for Re = 2,800. The shape of the cylinder cross section was exactly the same as that used in the experiments. The axial (spanwise) direction was assumed as homogeneous. The outer boundary of the computational domain was located ≈ 3 diameters (0.07 m) away from the center of rotation, and the axial size of the domain was ≈ 1 diameter (0.024 m).

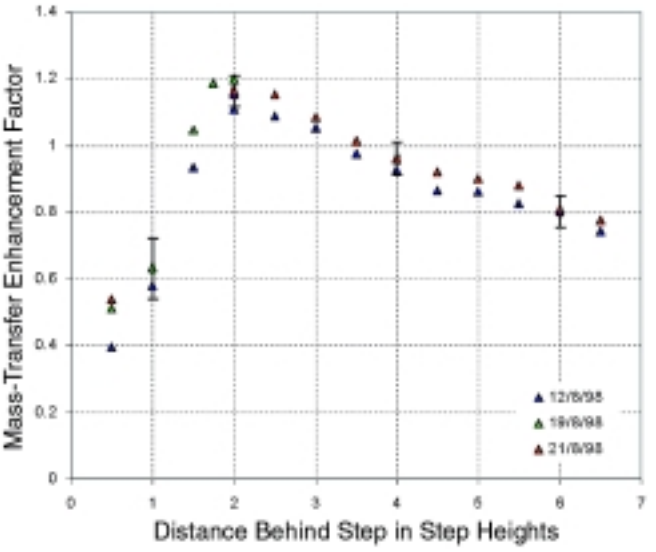

FIGURE 10. *Enhancement of mass transfer behind the step as a function of distance behind the step for 1,000 rpm (Re = 19,300).*

The computational grid used in this study is shown in Figure 11. Figure 11(a) exhibits the whole computational domain at one cross section in the axial direction, and Figure 11(b) is a magnified view of the grid close to the cylinder. Since the cross-section geometry is symmetric with respect to the center of rotation, only one half of the cross section was considered in the simulations. The grid is a body-fitted, O-grid system, which is the most suitable type of grid for this complicated geometry, with more resolution near the steps and solid boundaries. The number of grid points was refined progressively up to 224 by 128 by 80 (in the tangential, radial, and axial

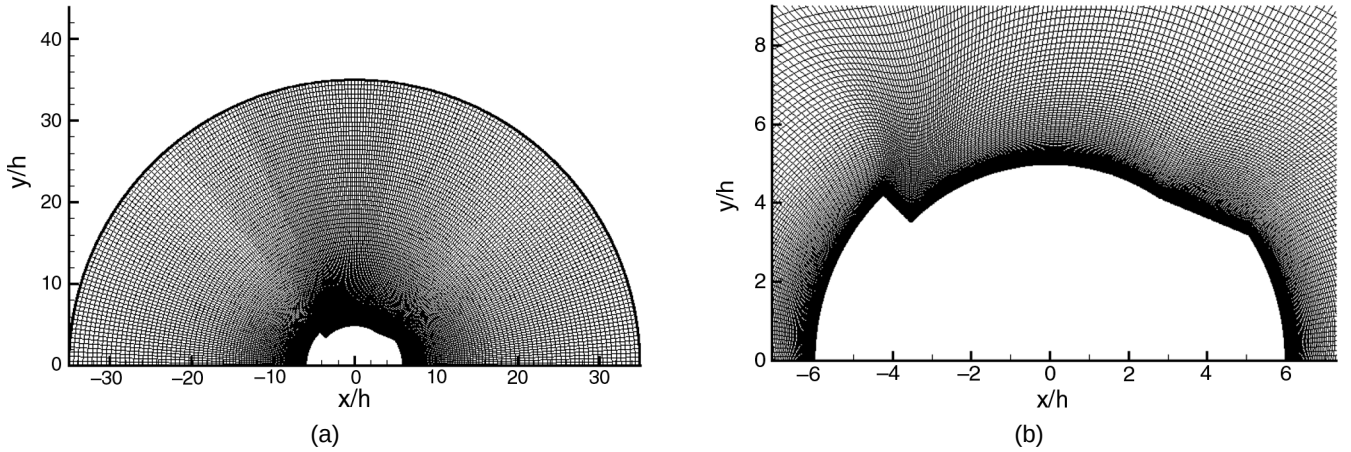

FIGURE 11. *Computational grid.*

directions, respectively). One typical run including statistical evaluation took ~ 12,000 time steps, which corresponds to 10 revolutions of the cylinder. One time step took ≈ 50 s of computation on a CRAY C90† supercomputer.

Initial and Boundary Conditions

With respect to the rotating reference frame, the inner cylinder is stationary while the outer circular boundary is rotating in the clockwise direction. The initial flow field was constructed such that, at any location in the flow field, the velocity was given as Ω times the distance between the point and the center of rotation (where Ω is the cylinder rotational speed in rad/s). This is an obvious choice because in the experiments, the cylinder started rotating in stationary surroundings. In addition, a small-amplitude random noise (with a root-mean-squared [rms] magnitude of ≈ 0.1% of the tangential speed of the cylinder surface) was added only at the beginning of the simulation to bypass the transitional regime and to establish a self-sustaining turbulence as quickly as possible.

The no-slip boundary condition was applied on the solid surfaces, and a periodic boundary condition was used in the tangential and axial directions. The outer boundary condition needed special attention. It seems most natural to impose a constant tangential speed of Ωr_0, where r_0 is the outer radius of the domain on the outer boundary. This corresponds to a practical situation where the outer solid boundary is located far away from the cylinder so that the fluid there is not disturbed by the motion of the cylinder. From the numerical point of view, this solution requires a large computational domain with a fine resolution near the outer boundary, which is not the region of interest. This would result in a significant waste of computational resources. To minimize such a waste, a "slip" boundary condition was devised and used on the outer boundary:

$$\frac{\partial u_\theta}{\partial n} = \Omega \qquad u_r = 0 \qquad \frac{\partial u_z}{\partial n} = 0 \tag{8}$$

where u_θ, u_r, and u_z represent the tangential, radial, and axial velocity components, respectively, and n denotes the direction locally perpendicular to the outer boundary (radial direction). This boundary condition allowed use of a reasonably small computational domain without significant disturbance of the flow field near the cylinder, which is the region of primary interest. Furthermore, since in this scheme the tangential velocity gradient is specified exactly at the boundary, rather than computed during the simulation, a fine numerical resolution was not required near the outer boundary, which led to additional saving in computational time.

RESULTS AND DISCUSSION

After the simulated flow pattern reached a statistically steady state, collecting hydrodynamic data for statistical evaluation was initiated. Averaging the flow field parameters was carried out in the homogeneous axial direction and in time. More than 160 data sets were collected over seven revolutions of the cylinder.

The mean velocity vector plot (averaged in time and the axial direction) in the vicinity of the step is shown in Figure 12. The main recirculating region and a secondary one near the corner can be identified clearly. A corresponding plot of the streamlines is shown in Figure 13. These two figures confirm the original expectation that this flow geometry will create a qualitatively similar flow pattern, as observed in a sudden pipe expansion or a plane backward-facing step, including flow separation and reattachment.

† Trade name.

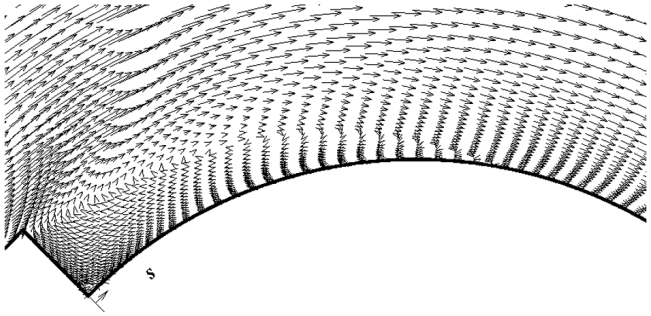

FIGURE 12. *Predicted mean velocity vector plot near the step (averaged in time and axial direction).*

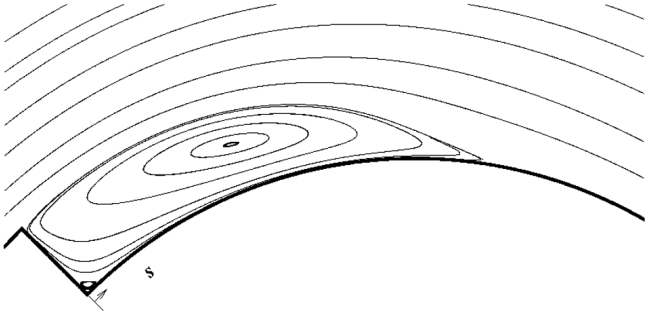

FIGURE 13. *Predicted mean streamlines near the step (averaged in time and axial direction).*

The transient flow simulations performed in the present work have shown that there is a large scale unsteadiness in the turbulent flow structure downstream the step not seen in time-averaged Figures 12 and 13. For example, the position of the instantaneous reattachment "point" fluctuates significantly—up to ≈ 3 step heights (3 h). This is a fact that was missed completely by all the standard k-ε turbulent flow simulations reported previously for similar flow geometries.[4] To illustrate this important point, images of the instantaneous flow pattern at the same axial plane but at two different times, ≈ 0.58 revolutions apart, is shown in Figure 14. The flow patterns were quite different as one can expect in turbulent flows. Similar behavior was reported by Le, et al., in the case of plane backward-facing step flow.[24] This large scale unsteadiness of the flow pattern downstream of the step can explain the relatively broad ("smeared") peaks in mass-transfer measurements shown in Figures 8 through 10.

The distribution of the mean tangential wall-shear stress and the rms of its fluctuation (both normalized with $1/2\rho U_\theta^2$) downstream the step is shown in Figure 15 (averaged in time and axial direction). The mean reattachment point of the main recirculating region where the wall shear stress is zero is located 4.9 h downstream the step. The largest mean wall shear stress occurred in the recirculating region at 2.9 h downstream the step. Another interesting feature is that the rms of the wall shear stress fluctuation was of the same order or larger than the mean value throughout the domain. The profile of the rms of the fluctuating wall shear stress peaked at 3.5 h downstream the step. This profile was remarkably similar to the measured mass-transfer profiles shown in Figures 8 through 10. However, any further direct comparisons were hampered by the discrepancy in the Reynolds numbers (simulated: Re = 2,800; measured: Re = 3,860, 9,650, and 19,300).

The mean total turbulence intensity also is shown in Figure 15 (values denoted on the secondary axis). It was computed as $\sqrt{\left(\overline{u_i' u_i'}/3\right)}$, where u_i' denotes

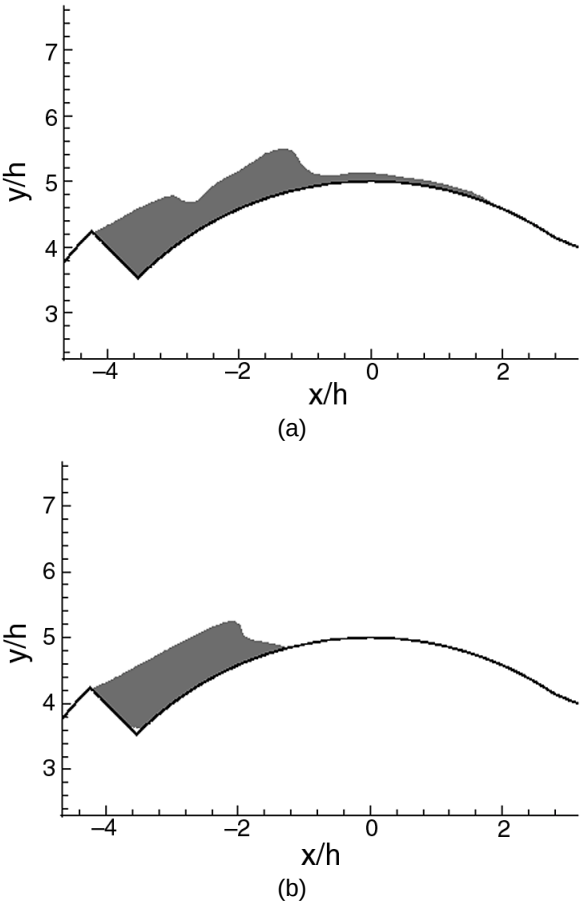

FIGURE 14. *Instantaneous flow pattern (dark color denoting the region of negative tangential velocity—i.e., reversed flow) at the same axial cross section and at two different times, ≈ 0.58 revolutions apart.*

velocity fluctuation in each direction (Einstein summation is assumed for repeated indices) and the overbar represents time and space averaging in the axial direction. Values taken at 0.006 h away from the wall were normalized with the cylinder peripheral tangential velocity (U_θ) as the characteristic velocity scale. A local maximum of the total turbulence intensity was found to be 1 step height upstream from the mean reattachment point (at 3.9 h down-

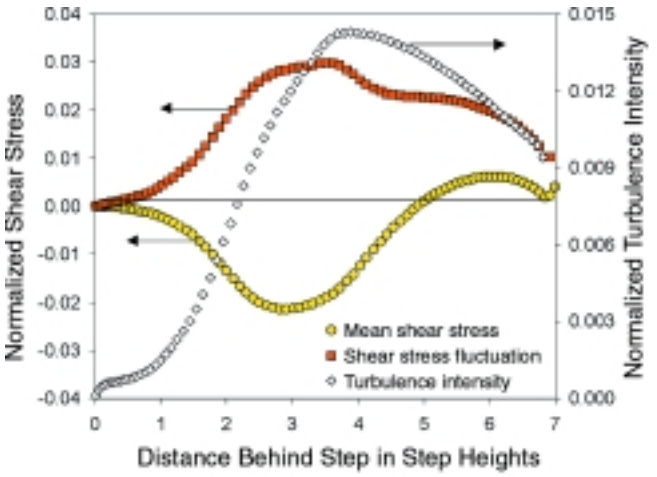

FIGURE 15. *Normalized distributions of the mean tangential wall shear stress, the rms of tangential wall shear stress fluctuation, and the mean total turbulence intensity at 0.006 h away from the cylinder surface (all averaged in time and axial direction) as a function of distance behind the step.*

stream the step). This is in contrast with previous reports that the two coincide in the case of flow through the sudden pipe expansion.[4,7]

CONCLUSIONS

❖ A new, compact experimental setup was tested intended for the study of erosion-corrosion under disturbed flow conditions, involving a rotating cylinder geometry with a sudden step.
❖ In this pilot study, a thorough characterization of the stepped rotating cylinder electrode was initiated, involving mass-transfer measurements complemented with direct numerical simulation of the turbulent flow around the new electrode.
❖ A large variation of the mass-transfer rates behind the step was measured similar in character to the one obtained in flow through a sudden pipe expansion.
❖ Flow simulations have confirmed that this flow geometry will create a qualitatively similar mean flow pattern as observed in a sudden pipe expansion or a plane backward-facing step flow.
❖ Further, simulations have shown that there is a large scale unsteadiness in the turbulent flow structure downstream the step, a fact completely missed by all the standard k-ε turbulent flow simulations reported previously for similar flow geometries, which might have a significant impact on erosion-corrosion.
❖ Further work on characterization of the new electrode involving erosion-corrosion measurements, numerical analysis of the complex flow structure, and the effect it has on erosion-corrosion are in progress. The authors believe that in the near future, this flow geometry will become an effective tool for studying erosion-corrosion under disturbed flow conditions and, in many cases, will become a substitution for much more complex and expensive flow loop-based systems.

ACKNOWLEDGMENTS

The experimental study was supported in part by an Australian Research Council grant. The computational part of the research was supported financially by 1998 CRAY R&D Research Fund in Korea and by a grant from The University of Queensland. Computations were carried out by using the CRAY C90† of the KORDIC supercomputer center in Korea.

REFERENCES

1. E. Heitz, Werkstoff. Korr. 15 (1964): p. 63.
2. E. Heitz, Corrosion 47 (1991): p. 135.
3. U. Lotz, J. Postlethwaite, Corros. Sci. 30 (1990): p. 95.
4. S. Nesic, J. Postlethwaite, Corrosion 46 (1990): p. 874.
5. B.C. Syrett, Corrosion 32 (1976): p. 242.
6. W. Blatt, E. Heitz, "Hydromechanical Measurements for Erosion-Corrosion," CORROSION/90, paper no. 25 (Houston, TX: NACE International, 1990).
7. S. Nesic, J. Postlethwaite, Can. J. Chem. Eng. 69 (1991): p. 698.
8. J.L. Dawson, C.C. Shih, "Corrosion Under Flowing Conditions—An Overview and Model," in Flow-Induced Corrosion, eds K.J. Kennelly, R.H. Hausler, D.C. Silverman (Houston, TX: NACE, 1991).
9. B.K. Mahato, S.K. Voora, L.W. Shemilt, Corros. Sci. 8 (1968): p. 173.
10. K.D. Efird, Corrosion 33 (1977): p. 3.
11. D.C. Silverman, "Rotating Cylinder Electrode—An Approach for Predicting Velocity Sensitive Corrosion," CORROSION/90, paper no. 13 (Houston, TX: NACE, 1990).
12. J.S. Newman, Electrochemical Systems, 2nd ed. (Englewood Cliffs, NJ: Prentice Hall, 1991).
13. D.R. Gabe, J. Appl. Electrochem. 4 (1974): p. 91.
14. D.R. Gabe, F.C. Walsh, J. Appl. Electrochem. 13 (1983): p. 3.
15. D.R. Gabe, G.D. Wilcox, J. Gonzalez-Garcia, J. Appl. Electrochem. 28 (1998): p. 759.
16. M. Eisenberg, C.W. Tobias, C.R. Wilke, J. Electrochem. Soc. 101 (1954): p. 306.
17. D.R. Gabe, P.A. Makanjuola, J. Appl. Electrochem. 17 (1987): p. 370.
18. J. Bienkowski, "A Rotating Cylinder Electrode with Surface Roughness" (Honours Thesis, The University Of Queensland, 1998).
19. W.H. Linton, T.K. Sherwood, Chem. Eng. Progr. 46 (1950): p. 288.
20. P. Van Shaw, L.P. Reiss, T.J. Hanratty, J. Amer. Inst. Chem. Eng. 9 (1963): p. 362.
21. T. Sydberger, U. Lotz, J. Electrochem. Soc. 129 (1982): p. 276.
22. D.K. Lezius, J.P. Johnston, J. Fluid Mech. 77 (1976): p. 153.
23. M. Rosenfeld, D. Kwak, M. Vinokur, J. Comput. Phys. 94 (1994): p. 102.
24. H. Le, P. Moin, J. Kim, J. Fluid Mech. 330 (1997): p. 349.